ADVANCED FUNCTIONAL MATERIALS
www.afm-journal.de

A Supermolecular Photosensitizer with Excellent Anticancer Performance in Photodynamic Therapy

Ruizheng Liang, Rui Tian, Lina Ma, Lele Zhang, Yanli Hu, Jian Wang, Min Wei, Dan Yan,* David G. Evans, and Xue Duan*

A supermolecular photosensitizer with excellent anticancer behavior when used for photodynamic therapy (PDT) is fabricated by the incorporation of zinc phthalocyanines (ZnPc) into the gallery of a layered double hydroxide (LDH). The composite material possesses uniform particle size (hydrodynamic diameter ~120 nm), and the host–guest and guest–guest interactions result in a high dispersion of ZnPc in a monomeric state in the interlayer region of the LDH matrix, with high singlet oxygen production efficiency. In vitro tests performed with HepG2 cells reveal a satisfactory PDT effectiveness of the ZnPc(1.5%)/LDH composite photosensitizer: a cellular damage as high as 85.7% is achieved with a rather low dosage of ZnPc (10 μg/mL). An extraordinarily high specific efficacy is demonstrated (31.59 μg^{-1} $(J/cm^2)^{-1}$), which is over 185.5% enhancement compared with the previously reported photosensitizers under similar test conditions. Furthermore, an in vivo study of the ZnPc(1.5%)/LDH demonstrates excellent PDT performance with an ultra-low dose (0.3 mg/kg) and a low optical fluence rate (54 J/cm^2). In addition, the ZnPc/LDH photosensitizer displays high stability, good biocompatibility, and low cytotoxicity, which would guarantee its practical application. Therefore, this work provides a facile approach for design and fabrication of inorganic–organic supermolecular materials with greatly enhanced anticancer behavior.

1. Introduction

Recently, photodynamic therapy (PDT) has attracted increasing attention in cancer therapy field owing to the advantages of effective and non-invasive treating diseased tissues while causing minimal damage to healthy tissues. Moreover, this method shows high efficiency in producing direct cellular death, vascular shutdown and immune activation, resulting in excellent therapeutic effects.[1–4] The principle of PDT involves the injection of photosensitizers at tumor sites, followed by light irradiation to generate singlet oxygen that induces cellular damage *via* apoptosis and/or necrosis.[5] The property of photosensitizer plays a key role in determining the PDT effectiveness, which has been regarded as the research focus of this area. The most commonly used photosensitizers are metallic phthalocyanines, owing to their intense absorption in the near-infrared region, long triplet lifetime, and high singlet oxygen quantum yield.[6] However, these photosensitizers generally suffer from weak hydrophility and low biocompatibility, which leads to unsatisfied PDT effect and therefore limits their further applications.[7]

To overcome these shortcomings, various nano-sized substrate materials including nanospheres, liposomes and polymeric micelles have been incorporated with metallic phthalocyanines to obtain composite photosensitizers, so as to improve the solubility and stability.[8] These composites exhibit prolonged circulation by avoiding rapid renal clearance and unwanted uptake, which result in enhanced PDT effectiveness.[9] However, serious aggregation or self-association of phthalocyanine molecules generally occurs in these composite systems, leading to reduced triplet yield and concomitant singlet oxygen production, as well as somewhat undesirable effects.[10] Therefore, to meet the requirements of high quality photosensitizers, the development of materials and strategies for the fabrication of new photosensitizer systems with excellent dispersibility and superior PDT efficiency remains a challenging goal.

Layered double hydroxides (LDHs) are a class of naturally occurring and synthetic materials generally expressed by the formula $[M^{2+}_{1-x}M^{3+}_{x}(OH)_2](A^{n-})_{x/n}\cdot mH_2O$, in which M^{2+} and M^{3+} cations are located in the brucite-like layers and A^{n-} is the charge-balancing interlayer anion.[11] By virtue of the versatility in chemical composition as well as the stability and biocompatibility of LDH materials, they have been widely explored in the fields of drug/gene delivery and inorganic-biology composite

R. Liang, R. Tian, Prof. M. Wei, Prof. D. G. Evans, Prof. X. Duan
State Key Laboratory of Chemical Resource Engineering
Beijing University of Chemical Technology
Beijing 100029, PR China
Fax: (+86)10–6442–5385
E-mail: weimin@mail.buct.edu.cn

L. Ma, L. Zhang, Dr. D. Yan
Military Institute of Chinese Materia Medica
302th Military Hospital of China
Beijing 100039, PR China
E-mail: yd277@126.com

Y. Hu, Prof. J. Wang
Fujian Provincial Key Laboratory of Analysis and Detection for Food Safety
Department of Chemistry
Fuzhou University
Fujian 350002, PR China

DOI: 10.1002/adfm.201303811

materials.[12] In our previous work, we have demonstrated that the intercalation of organic dyes into LDH interlamellar gallery can effectively depress the aggregation, enhance the dispersion and stability of the guests.[13] This therefore motivates us to take the challenge of fabricating phthalocyanines/LDH composite photosensitizers by incorporation of phthalocyanine molecules into LDH matrix, which would exhibit the following advantages: (i) the host-guest interactions (e.g., the electrostatic, van der Waals interaction, or hydrogen bonding) induce a homogeneous distribution of phthalocyanine guests at the molecular level, which would increase the singlet oxygen quantum yield; (ii) the LDH matrix promotes the hydrophility and biocompatibility of organic photosensitizers, resulting in enhanced drug permeability/retention. Moreover, the chemical stability and photostability of the phthalocyanines can be largely-improved by the introduction of inorganic LDH component.

In this work, we report a new supermolecular photosensitizer by incorporation of zinc phthalocyanines (ZnPc) into the LDH gallery, which show extraordinarily high anticancer behavior in PDT as well as low cytotoxicity. XRD and UV-vis spectroscopy confirm that the ZnPc molecules are accommodated in the interlayer region of LDH matrix with monomer state. The composite material possesses uniform particle size with the equivalent hydrodynamic diameter of ~120 nm. In vitro tests performed with HepG2 cell reveal a satisfactory PDT effectiveness of the ZnPc(1.5%)/LDH composite photosensitizer: a cellular damage as high as 85.7% was achieved with a very low dosage of ZnPc (10 μg/mL). Moreover, its specific efficacy is rather high (31.59 $\mu g^{-1}(J/cm^2)^{-1}$), over 185.5% increase compared with the previously reported photosensitizers. In vivo tests of ZnPc(1.5%)/LDH-induced anticancer behavior demonstrate an excellent PDT performance with an ultra-low dose of 0.3 mg/kg and low optical fluence rate of 54 J/cm^2. The high dispersion of ZnPc in the LDH gallery inhibits its aggregation, and the suitable particle size and biocompatibility of the ZnPc/LDH composite facilitate the drug delivery, accounting for the excellent PDT performance. Additionally, the ZnPc/LDH photosensitizer displays high stability, good biocompatibility as well as low cytotoxicity, which would guarantee its practical applications.

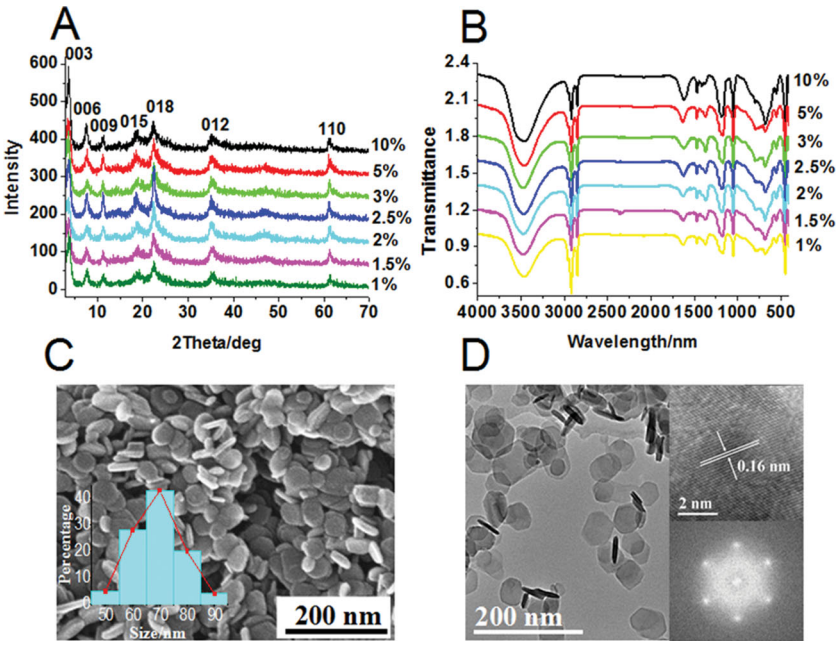

Figure 1. (A) The XRD patterns and (B) FT-IR spectra of various ZnPc(*x*%)/LDH composites with *x*% ranging from 1% to 10%. (C) SEM image of the ZnPc(1.5%)/LDH sample with particle size distribution shown in the inset. (D) TEM of the ZnPc(1.5%)/LDH sample; the insets display the lattice fringe and Fourier transform image.

2. Results and Discussion

2.1. Structural and Morphological Characterization

ZnPc and SDS were co-intercalated into the interlayer region of LDH, in which SDS serves as a dispersant for controlling the loading and distribution of ZnPc. The XRD patterns of ZnPc(*x*%)/Mg_2Al-LDH samples are shown in **Figure 1**A and Figure S1A. In each case, the XRD pattern exhibits the characteristic reflections of the LDH layered structure with a series of (00*l*) peaks appearing as narrow, strong lines at low angle, indicating the guests have been successfully intercalated into the LDH gallery to produce a supermolecular structure. The basal spacing (d_{003}) of ZnPc (*x*%)/Mg_2Al-LDH (Figure S1B) ranges in 23.6–24.6 Å with *x*% varies in 1–10%, which can be attributed to the change in guest orientation resulting from different ratios of SDS/ZnPc. The co-intercalation of ZnPc and SDS anions was further confirmed by the corresponding FT-IR spectra (Figure 1B, Figure S2). The absorption bands at 2923 and 2853 cm^{-1} are assigned to the asymmetric $\nu_{as}(CH_2)$ and symmetric $\nu_s(CH_2)$ vibration of SDS; while the bands at 1609, 1190 and 1032 cm^{-1} are characteristic of the C=C bond of benzene ring in ZnPc.[14] The results (Figure 1B) also show that the intensity of ZnPc characteristic peaks (1609, 1190 and 1032 cm^{-1}) increases gradually along with the enhancement of ZnPc amount (from 1% to 10%). The presence of SDS in the ZnPc(*x*%)/Mg_2Al-LDH imposes a dilution effect and thus inhibits the aggregation of ZnPc (**Scheme 1**). The chemical compositions of the resulting products measured by inductively coupled plasma atomic emission spectroscopy (ICP-AES) are listed in Table S1, from which the determined ZnPc

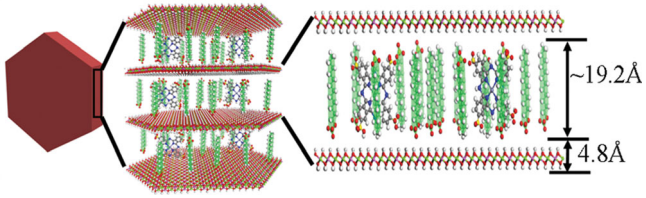

Scheme 1. Schematic illustration of the ZnPc(*x*%)/LDH structure.

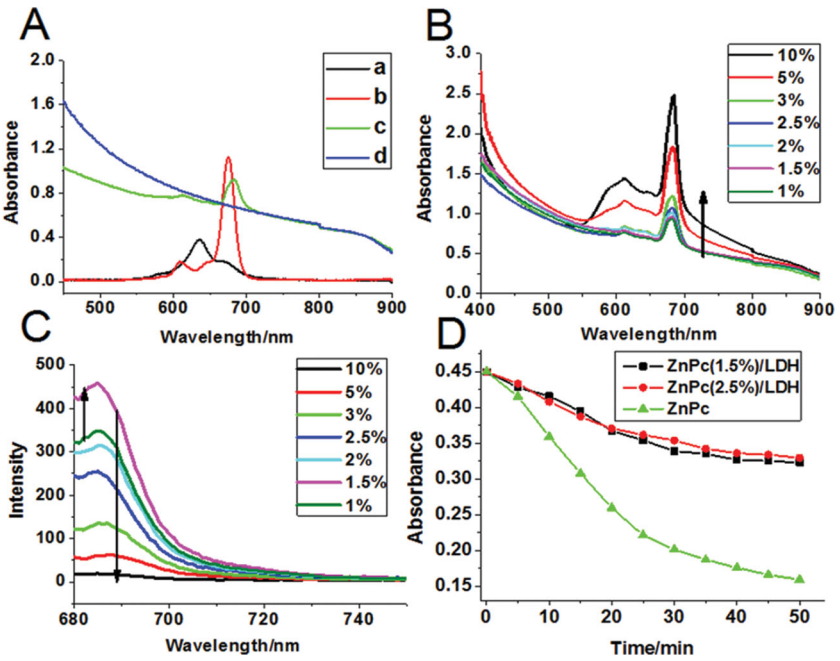

Figure 2. (A) The UV-vis absorption spectra of: (a) pristine ZnPc (2×10^{-5} M) in aqueous solution, (b) pristine ZnPc (2×10^{-5} M) in 60% ethanol solution, (c) ZnPc(1.5%)/LDH (3×10^{-4} M) aqueous suspension, (d) pristine LDH (3×10^{-4} M) aqueous suspension. (B) The UV-vis absorption spectra and (C) photoluminescence spectra of various ZnPc(*x*%)/LDH suspension (3×10^{-4} M) with *x* ranging in 1–10%. (D) Decay curves of absorption at 678 nm for ZnPc(1.5%)/LDH, ZnPc(2.5%)/LDH and 635 nm for pristine ZnPc, respectively, as a function of irradiation time (650 nm).

content (*x*%) is close to the nominal value. SEM (Figure 1C) and TEM (Figure 1D, Figure S3) image show that the sample of ZnPc(1.5%)/Mg_2Al-LDH possesses uniform plate-like morphology with particle size ranging in 60–80 nm; the lattice fringe of 0.16 nm can be attributed to the (110) plane of the LDH phase (Figure 1D). Moreover, the equivalent hydrodynamic diameter of ZnPc(1.5%)/Mg_2Al-LDH in aqueous solution was determined to be ~120 nm (Figure S4).

The as-prepared ZnPc(*x*%)/LDH samples show interesting optical properties which are different from pristine ZnPc. Pristine ZnPc prefers to exist as the dimer or multimer (H-type aggregates) in high polarity media (*e.g.* aqueous solution), with contiguous ZnPc molecules in a co-facial arrangement.[15] An absorption maximum of 635 nm was observed for the ZnPc aqueous solution (**Figure 2**A, curve a); while it presents in monomer state in ethanol solution and the absorption maximum moves to 675 nm (Figure 2A, curve b; Figure S5). The red-shift of the ZnPc Q-band indicates the collapse of the H-type aggregation in low polarity media. In the case of the ZnPc(1.5%)/LDH aqueous suspension, an absorption maximum at 678 nm was observed (Figure 2A, curve c), indicating the LDH gallery provides a low polarity microenvironment for the formation of monomeric ZnPc. Furthermore, the effect of ZnPc loading on the ZnPc(*x*%)/LDH samples was further investigated and the absorption spectra is shown in Figure 2B. With the increase of ZnPc loading from 1% to 10%, the intensity of absorption maximum at 678 nm enhances gradually; however, a broad absorption band in 580–610 nm appears with increasing intensity as the ZnPc content rises from 2.5% to 10%, which could be ascribed to the formation of some co-facial aggregation state of ZnPc molecules.

Figure 2C displays the photoluminescence (PL) spectra of ZnPc(*x*%)/LDH materials with various ZnPc loading. The fluorescence intensity increases at first to a maximum and then decreases along with the enhancement of ZnPc content from 1% to 10%. The optimal luminous intensity presents in the sample with 1.5% ZnPc. ZnPc exhibits the monomer molecular luminescence with low concentration, accounting for the increase in the luminous intensity firstly (from 1% to 1.5%); the H-type aggregate comes into formation as the ZnPc content surpasses a certain value (from 2% to 10%), resulting in the subsequent fluorescence quenching. Based on the chemical composition of ZnPc(1.5%)/LDH (Table S1) and its unit cell parameter *a* ($a = 2d_{110} = 2.99$ Å), the average distance between two adjacent ZnPc monomers in the interlayer region was calculated to be ~2.8 nm. Moreover, the effect of the host layer on the PL emission was further studied (Figure S6), and both the absorption at 678 nm and fluorescent intensity at 86 nm obey the following order: Mg_2Al > Mg_3Al > Zn_2Al = Zn_3Al-LDH (Figure S7). The results above indicate that both the host–guest interaction (composition and charge density of LDH layer) and the guest–guest interaction (ZnPc loading) are key factors in determining the luminous property of ZnPc within the LDH matrix. The absorption and luminous behavior of ZnPc/LDH composites correlate closely with the triplet yield and singlet oxygen production, which further determines the PDT performance. In addition, Figure 2D shows the photostability of ZnPc/LDH composite in comparison with pristine ZnPc. After continuous irradiation under 650 nm for 50 min, the absorbance of pristine ZnPc decreases 64.4% while only 28.9% and 26.7% loss were found for ZnPc(1.5%)/LDH and ZnPc(2.5%)/LDH, respectively. This indicates that the ZnPc/LDH system possesses a better resistance against photobleaching than pristine ZnPc.

2.2. Measurements of Singlet Oxygen and In Vitro PDT Performance

We further measured the singlet oxygen production efficiency of ZnPc(*x*%)/LDH, which is the key factor of PDT performance. A chemical method using 1,3-diphenylisobenzofuran (DPBF) as a detector (absorption band: 410 nm) was carried out to assess the singlet oxygen production of ZnPc(*x*%)/LDH, based on the irreversible reaction between DPBF and singlet oxygen which induces a decrease in the absorption at 410 nm. **Figure 3** and Figure S8 show the absorption intensity of DPBF at 410 nm with the presence of various samples as a function of exposure time under 650 nm. The slope of the curve is proportional to the efficiency of produced singlet oxygen.

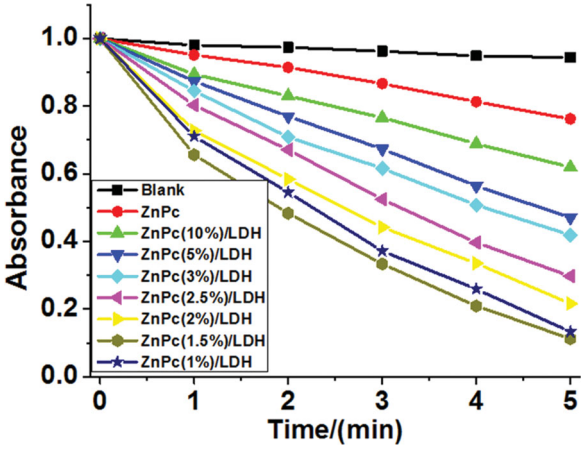

Figure 3. The normalized decay curves for absorption of DPBF at 410 nm as a function of irradiation time (under 650 nm), in the presence of pristine ZnPc, ZnPc(*x*%)/LDH as well as blank measurement.

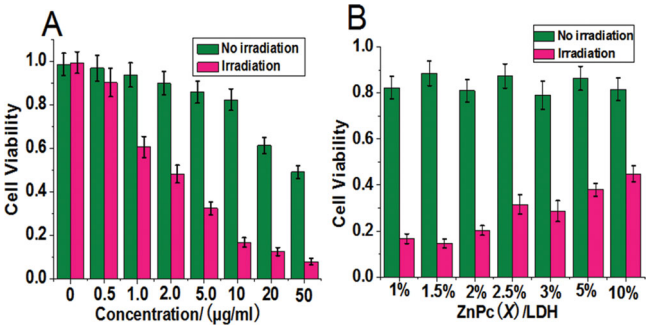

Figure 4. The PDT performance of (A) ZnPc(1%)/LDH with various concentrations after 24 h incubation; (B) ZnPc(*x*%)/LDH with the concentration of equivalent ZnPc (10 μg/mL) after 24 h incubation (*x* ranges in 1–10%). Red and green columns denote the results under irradiation and without irradiation, respectively. HepG2 cells were used in these cases.

For the DPBF solution, a rather slow decrease in absorbance at 410 nm was observed upon irradiation, owing to its self-decomposition (Figure 3). The presence of pristine ZnPc accelerates this process, indicating DPBF reacts with the singlet oxygen generated by ZnPc. In the case of ZnPc(*x*%)/LDH materials, a sharp decrease in absorbance was observed within 5 min. The singlet oxygen production of ZnPc(*x*%)/LDH increases at first to a maximum (1.5%) and then decreases along with the enhancement of ZnPc loading, which indicates the sample of ZnPc(1.5%)/LDH exhibits the strongest capability to produce singlet oxygen. This result originates from the highest density of ZnPc monomer in this sample, in well accordance with its luminous intensity (Figure 2C) discussed above. After a 5 min irradiation, a decrease of 89% in the absorbance was observed for ZnPc(1.5%)/LDH; while only 24% was found for pristine ZnPc. It is therefore concluded that monodisperse ZnPc in the LDH gallery plays a key role in boosting the production of singlet oxygen.

The PDT performance of ZnPc(*x*%)/LDH composite photosensitizers was further studied by in vitro tests performed with HepG2 cells. The impact of ZnPc/LDH dosage on PDT effectiveness was firstly explored. The HepG2 cells were incubated in the presence of ZnPc(1%)/LDH suspension with different concentrations for 24 h, followed by washing with PBS and irradiated at 650 nm with 27 J/cm^2 (15mW/cm^2, 0.5 h). **Figure 4**A displays the comparison study of cell viability between with and without irradiation. A significant PDT effect occurs and enhances gradually along with the increase of dosage. The best PDT behavior was demonstrated with the dosage of 10 μg/ml (the difference between the green and red bar: 0.66), although some cytotoxicity occurs with this dosage. The ZnPc loading in the ZnPc(*x*%)/LDH composites (x = 1–10%) with the concentration of equivalent ZnPc (10 μg/mL) was further investigated (Figure 4B), from which obvious difference in the PDT performance in this range was observed. The maximum difference between irradiation and no irradiation presents in the sample of ZnPc(1.5%)/LDH (the difference value: 0.74). The results approximatively accord with the singlet oxygen production efficiency of these ZnPc(*x*%)/LDH composite photosensitizers. In order to make a comparison of PDT performance between this work and previous reports, we denoted specific efficacy as the number of dead cells induced per μg/mL of photosensitizer and per J/cm^2 optical fluence rate. It should be noted that the ZnPc(1.5%)/LDH composite exhibits a rather high specific efficacy (31.59 μg^{-1}(J/cm^2)$^{-1}$), which is over 185.5% enhancement compared with the previously reported photosensitizers under similar test conditions (Table S2).

For comparison, the PDT performance of pristine ZnPc (10 μg/mL), SDS (0.5 mg/mL) and LDH (0.5 mg/mL) was also studied by incubating HepG2 cells in these media respectively (Figure S9). The blank test shows that the irradiation imposes no influence on the cell viability. The sample of LDH does not show both PDT effect as well as cytotoxicity, demonstrating its biocompatibility as reported previously. For SDS, although no PDT effect but somewhat cytotoxicity was observed, it is essential to achieve the dispersion of ZnPc molecules in the interlayer region of LDH matrix with monomer state. For the sample of pristine ZnPc, the cell viability is 0.81 (no irradiation) and 0.66 (irradiation), indicating some cytotoxicity as well as rather poor PDT effectiveness. In the case of ZnPc(1.5%)/LDH sample (Figure 4B), the cell viability is found to be 0.89 (no irradiation) and 0.15 (irradiation) respectively, which demonstrates largely-enhanced PDT effectiveness and acceptable cytotoxicity. Moreover, Figure S10 shows the fluorescence microscopy images of HepG2 cells treated with ZnPc(1.5%)/LDH for 0 h and 24 h incubation without washing, respectively. Numerous photosensitizer particles were attached to the cell surface at 0 h; while a significant decrease in the particle number was observed after 24 h incubation, indicating that the photosensitizer particles can enter into HepG2 cells during the incubation process.

In order to visualize the phototoxicity results, the presence of dead cells after PDT was evaluated by staining with propidium iodide (PI), which is excluded by viable cells but can penetrate into the cell membrane of dead cells. We firstly studied the cytotoxicity of photosensitizers with the absence of irradiation. HepG2 cells treated with 10 μg/mL of ZnPc(1%)/LDH, ZnPc(1.5%)/LDH, ZnPc and blank without irradiation are displayed in **Figure 5**A–D. After incubation for 24 h, pristine ZnPc leads to remarkable cell mortality (Figure 5B); while ZnPc(1%)/LDH and ZnPc(1.5%)/LDH only induce somewhat cell

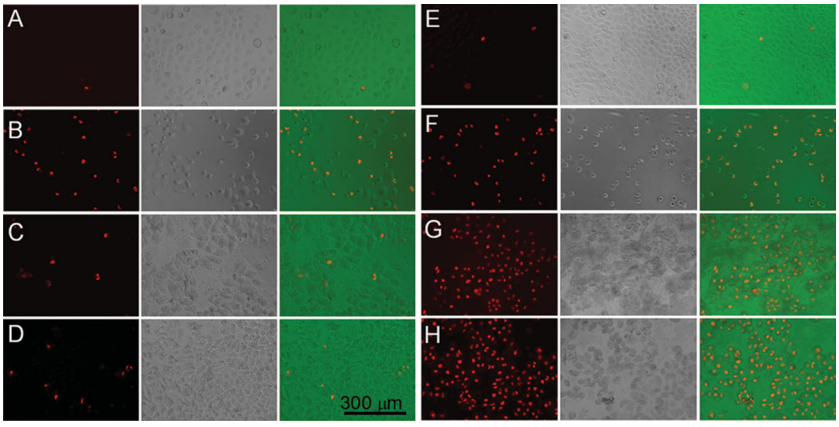

Figure 5. Fluorescence microscopy (left column), bright field (middle column) and merged (right column) images of HepG2 cells treated with various photosensitizers without irradiation (10 μg/ml, 24 h incubation): (A) blank, (B) ZnPc, (C) ZnPc(1%)/LDH, (D) ZnPc(1.5%)/LDH. HepG2 cells treated with various photosensitizers under irradiation (10 μg/ml, 24 h incubation): (A) blank, (B) ZnPc, (C) ZnPc(1%)/LDH, (D) ZnPc(1.5%)/LDH.

mortality (Figure 5C and D). Subsequently, the PDT behavior of these photosensitizers was further investigated under irradiation (650 nm). The fluorescence microscopy image of blank experiment shows that HepG2 cells with 24 h incubation (Figure 5E) have no obvious apoptosis upon irradiation. The addition of ZnPc (10 μg/mL) causes partial apoptosis for 24 h incubation (Figure 5F), indicating a weak PDT performance. In contrast, the cells treated with ZnPc(1%)/LDH photosensitizer (10 μg/mL) exhibit intense PI signal (Figure 5G), indicating most cells were dead after light irradiation regardless of incubation. Cells treated with ZnPc(1.5%)/LDH (10 μg/mL) also display a similar situation (Figure 5H). The results show that the ZnPc/LDH composite photosensitizers display superior PDT effectiveness, high stability as well as low cytotoxicity.

2.3. Fluorescence Imaging and In Vivo PDT Performance

In vivo PDT performance of the ZnPc(1.5%)/LDH photosensitizer was further studied on male Balb/c mice from the viewpoint of practical applications. Firstly, 20 μL of ZnPc(1.5%)/LDH (0.4 mM) was injected into the tumor site (60 mm^3) of mice, and in vivo fluorescence imaging was recorded on a Carestream Molecular Imaging In-Vivo MS FX PRO system. As shown in **Figure 6**A, the intratumoral injection site displays a strong fluorescence signal (0 h). The area of the fluorescence signal expands from center along with the prolongation of time (0–4 h), indicating a good distribution ability of ZnPc(1.5%)/LDH in tissue. The average fluorescence intensity of ZnPc(1.5%)/LDH acquired in the tumor area remains rather strong within 4 h post-injection followed by fast decrease. The results show that ZnPc(1.5%)/LDH can be used as a good photosensitizer for in vivo PDT treatment. Taking into account both the NIR fluorescence imaging

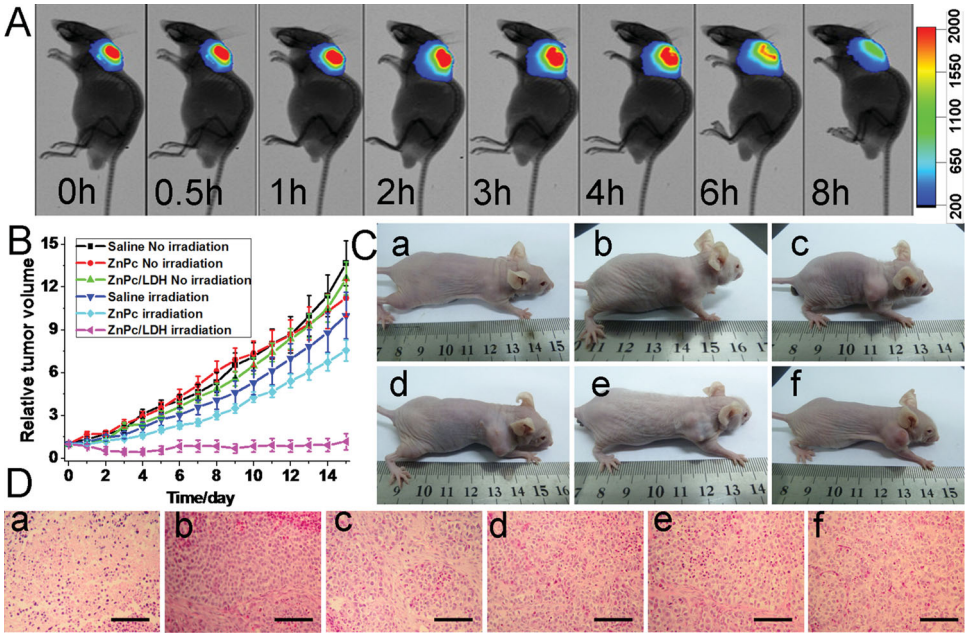

Figure 6. (A) In vivo fluorescence imaging of mice after intratumoral injection with 20 μL of ZnPc(1.5%)/LDH at different time points (0 h, 0.5 h, 1 h, 2 h, 3 h, 4 h, 6 h, 8 h). (B) The tumor growth curves of the six groups of mice after treatment. The tumor volume was normalized to the initial size; the error bar was based on standard deviation of mice per group. (C) Representative photos of mice bearing HepG2 tumors after various treatments (a: ZnPc(1.5%)/LDH, 54 J/cm^2; b: ZnPc, 54 J/cm^2; c: saline, 54 J/cm^2; d: ZnPc(1.5%)/LDH only; e: ZnPc only; f: saline only). (D) H&E stained tumor slices collected from the six groups after 24 h of various treatments (a–f: the same to C; the scale bar is 200 μm). The tumor with ZnPc(1.5%)/LDH injection and irradiation was severely damaged.

observation and the irradiation time, 2 h after photosensitizer injection was selected as the suitable time point to implement PDT.

We further evaluated the in vivo therapeutic efficacy of ZnPc/LDH-induced PDT cancer treatment. Six groups of HepG2 tumor-bearing mice (8 animals per group) were employed in this work. For the target group, tumors were intratumorally injected with ZnPc(1.5%)/LDH (dosage: 0.3 mg/kg) and then irradiated by a simulated sunlight source (optical filter 650 ± 5 nm) with a power density of 30 mW/cm^2 for 30 min (fluence rate: 54 J/cm^2). Other control groups consist of saline injection with or without irradiation, ZnPc injection with or without irradiation, ZnPc(1.5%)/LDH injection without irradiation. The tumor size was measured by a caliper every day after treatment. It was found from Figure 6B that the in vivo PDT efficiency increases by the following order: saline (No irradiation) ≈ ZnPc (No irradiation) ≈ ZnPc(1.5%)/LDH (No irradiation) < saline (Irradiation) < ZnPc (Irradiation) < ZnPc(1.5%)/LDH (Irradiation). The ZnPc(1.5%)/LDH composite photosensitizer exhibits the most superior in vivo PDT behavior, i.e., the growth speed of tumor is restrained to a great extent. This striking contrast can be further visualized by the mice photograph after treatment of 15 days (Figure 6C). In addition, haematoxylin and eosin (H&E) staining of tumor slices was also carried out collected one day after treatment for all the six groups (Figure 6D). As expected, significant cancer cell damage was noticed in the tumor with ZnPc(1.5%)/LDH injection and irradiation (Figure 6D: a); while no obvious necrosis/apoptosis can be observed in other five control groups (Figure 6D: b–f). The results clearly demonstrate that ZnPc(1.5%)/LDH can serve as a powerful photosensitizer for in vivo PDT treatment of tumor, with a dose of 0.3 mg/kg and an optical fluence rate of 54 J/cm^2. Both the drug dose and optical power in this work are much lower than those of previous reports, in which a dose of 2–3 mg/kg and an optical fluence rate of 60–150 J/cm^2 are required to achieve substantial in vivo treatment efficacy.[16] The excellent anticancer performance of ZnPc/LDH in vivo makes it an encouraging agent in PDT area, which would guarantee its practical application.

3. Conclusions

A supermolecular photosensitizer used in PDT was fabricated by incorporation of ZnPc into a LDH gallery. The host-guest and guest-guest interactions result in the high dispersion of ZnPc as monomeric state in the interlayer region of LDH matrix, with a large singlet oxygen production efficiency. *In vitro* tests performed with HepG2 cells reveal that the ZnPc/LDH composite photosensitizers exhibit a satisfactory PDT effectiveness, high stability, good biocompatibility as well as low cytotoxicity, in comparison with pristine ZnPc. In addition, the rather low dosage of ZnPc (10 μg/ml) accompanied with superior PDT behavior is the most distinct feature of this composite photosensitizer. In vivo tests demonstrate an excellent ZnPc/LDH-induced PDT behavior, with an ultra-low dose of 0.3 mg/kg and a low optical fluence rate of 54 J/cm^2. Therefore, this work provides a facile approach for design and fabrication of inorganic-organic supermolecular materials with largely-enhanced anticancer behavior by distributing ZnPc within an LDH layered matrix, which can serve as a promising photosensitizer in the field of PDT.

4. Experimental Section

Preparation of ZnPc(x%)/LDH: series of ZnPc(*x*%)/Mg_2Al-LDH composite materials were synthesized by a nucleation/crystallization separation method reported by our group. In brief, solution A: $Mg(NO_3)_2{\cdot}6H_2O$ (0.05 mol), $Al(NO_3)_3{\cdot}9H_2O$ (0.025 mol), sodium dodecyl sulfonate (SDS) (*a* mol) and ZnPc (*b* mol, in which $a + b = 0.025$ mol; *a*: *b* = 99:1; 98.5:1.5; 98:2; 97.5:2.5; 97:3; 95:5; 90:10, respectively; $x\% = b/(a + b)$) dissolved in 100 mL of ethanol solution (2:3, v/v). Solution B: NaOH (0.15 mol) dissolved in 100 mL of deionized water. Solution A and solution B were simultaneously added into a colloid mill rotating at 3000 rpm, and mixed for 1 min. The resulting slurry was removed from the colloid mill and was sealed in a Teflon-lined stainless steel autoclave and heated at 80 °C for 1 day. The product was washed with hot, distilled water and anhydrous ethanol thoroughly and then dried in vacuum at 60 °C for 6 h.

Detection of Singlet Oxygen: the generation of singlet oxygen for the ZnPc(*x*%)/LDH photosensitizer was detected chemically using 1,3-diphenylisobenzofuran (DPBF) as a singlet oxygen sensor.[17] The ZnPc(*x*%)/LDH suspension was prepared by dispersing ZnPc(*x*%)/LDH in acetonitrile (concentration: 30 μg/mL) and stored in the dark. A DPBF solution (15 μL, 59.5 μM) was added into the photosensitizer suspension (2 mL) and mixed throughly, followed by irradiation at 650 nm using a simulated sunlight source with optical filter 650 ± 5 nm. The decrease rate of the UV absorption intensity at 410 nm is proportional to the amount of singlet oxygen produced and the absorbance value was recorded per minute.

In vitro Studies on Tumor Cells: HepG2 cells were grown and expanded in 25 cm^2 cell-culture flask. After reaching 80~90% confluence, the HepG2 cells were washed with PBS, afterwards detached from the flask by addition of 1.0 mL of 0.25% trypsin for 1–3 min at 37 °C. HepG2 cells (1×10^4 cells/well) were seeded into two 96-well plates, respectively. The cells were then treated with ZnPc(*x*%)/LDH suspension. After a further incubation of 24 h, one plate was irradiated with a simulated sunlight source (optical filter 650 ± 5 nm) and another was stored in the dark. The colorimetric 3-(4,5-dimethylthiazol-2-yl)-2,5-diphenyltetrazolium bromide (MTT) was used to determine the cell viability.

To study the phototoxicity effect, HepG2 cells (1×10^4 cells/well) were seeded into two 96-well plates and then treated respectively with ZnPc(*x*%)/LDH (*x* = 1–10%, equivalent ZnPc (10 μg/ml), ZnPc (10 μg/ml), SDS (0.5 mg/ml), LDH (0.5 mg/ml) suspension/solution. After a further incubation of 24 h, cells were washed with PBS. One plate was irradiated with a simulated sunlight source (optical filter: 650 ± 5 nm; power density: 15 mW/cm^2) for 30 min and another was kept in the dark outside the incubator. The colorimetric MTT was used to determine the cell viability.

In a typical cellular image experiment, the cells (1×10^4 cells/well) were seeded into two 96-well plates respecitvely and incubated for 24 h. The cells were treated with 10 μg/ml of ZnPc(1%)/LDH, ZnPc(1.5%)/LDH, pristine ZnPc and blank, and then incubated at 37 °C for another 24 h. After washing with PBS and irradiation for 0.5 h, treated cells were stained with propidium iodide (PI) and mounted for optical microscope examinations. Cells which were treated with the same procedure but without irradiation were also studied as a reference sample.

Animal Experiments: Male Balb/c mice (Balb/c-nu, ~25 g) were purchased from Academy of Military Medical Science and used under protocols approved by 302nd Military Hospital Animal Research Center. $2{\times}10^5$ HepG2 cells suspended in 20 μL phosphate buffered saline (PBS) were subcutaneously injected into the right shoulder of each male Balb/c mouse. The mice bearing HepG2 tumors were treated when the tumor volume reached ~60 mm^3.

In vivo Photodynamic Therapy: Mice were randomized into six groups of 8 animals per group for the following treatments: (Group i) 20 μL of saline injected intratumorally without irradiation; (Group ii) 20 μL

of 0.4 mM ZnPc injected intratumorally without irradiation; (Group iii) 20 μL of ZnPc(1.5%)/LDH (equivalent 0.4 mM ZnPc) injected intratumorally without irradiation; (Group iv) 20 μL of saline injected intratumorally with irradiation at 54 J/cm^2; (Group v) 20 μL of 0.4 mM ZnPc injected intratumorally with irradiation at 54 J/cm^2; (Group vi) 20 μL of ZnPc(1.5%)/LDH (equivalent 0.4 mM ZnPc) injected intratumorally with irradiation at 54 J/cm^2. Mice with the PDT were irradiated with a simulated sunlight source (optical filter: 650 ± 5 nm; power density: 30 mW/cm^2) for 30 min (i.e., an optical fluence rate of 54 J/cm^2). The tumor size was measured by a caliper every day and calculated as the volume = (tumor length) × (tumor width)^2 × 0.5.[18] Relative tumor volume was calculated as V/V_0 (V, V_0 are the tumor volume measured at time t and t_0, respectively).

NIR Fluorescence Images and Histology Examination: For in vivo NIR fluorescence imaging, the mice were received intratumoral injection of the ZnPc(1.5%)/LDH solution with a dose of 0.3 mg/kg. NIR fluorescence images were obtained at 0, 0.5, 1, 2, 3, 4, 6 and 8 h after injection. For histological examination, tumors from the treated group and control groups were fixed in 4% formalin and conducted with paraffin embedded sections for H&E staining. The slices were examined by a digital microscope (Olympus).

Sample Characterization: Powder X-ray diffraction patterns of the samples were collected on a Shimadzu XRD-6000 diffractometer using a Cu Kα source, with a scan step of 0.02° and a scan range between 3° and 70°. The morphology of the samples was investigated using a scanning electron microscope (SEM; Zeiss SUPRA 55) with an accelerating voltage of 20 kV. Transmission electron microscopy (TEM) images were recorded with Philips Tecnai 20; the accelerating voltage was 200 kV. The chemical composition of LDH samples were determined by inductively coupled plasma (ICP) emission spectroscopy on a Shimadzu ICPS-7500 instrument. The particle size distribution was determined using a Malvern Mastersizer 2000 laser particle size analyzer. The Fourier transform infrared (FT-IR) spectra were recorded using a Vector 22 (Bruker) spectrophotometer using the KBr pellet technique in the range 4000–400 cm^{-1} with 2 cm^{-1} resolution. The solid UV-vis absorption spectra were collected in the range 200–900 nm on a Shimadzu U-3000 spectrophotometer, with a slit width of 1.0 nm. The fluorescence spectra were performed on a RF-5301PC fluorospectrophotometer with the excitation wavelength of 675 nm. The fluorescence emission spectra range in 680–750 nm, and the width of both the excitation and emission slit is 3 nm. Fluorescence images of these samples were obtained using an Olympus 1×71 fluorescence microscope with 400 folds enlargement. NIR fluorescence images were obtained using an IVIS Lumina fluorescence imaging system (Cy5.5 channel, λ_{ex} = 615–665 nm, λ_{em} = 695–770 nm).

Supporting Information

Supporting Information is available from the Wiley Online Library or from the author. It includes XRD profiles of the ZnPc(%)/MgAl-LDH (Figure S1); FT-IR spectra of SDS, ZnPc and SDS/LDH (Figure S2); TEM image of the SDS-ZnPc(1.5%)/LDH (Figure S3); Particle size distribution of ZnPc(1.5%)/LDH (Figure S4); The UV-vis absorption spectra of pristine ZnPc (Figure S5); SEM images, UV-vis absorption spectra and photoluminescence spectra of ZnPc(1.5%)/MAl-LDH (Figure S6-S7); The decay curves of absorption of DPBF in the presence of ZnPc(%)/LDH, ZnPc and blank as a function of irradiation time (Figure S8); The PDT performance of pristine ZnPc, SDS, LDHs and blank test (Figure S9); Fluorescence microscopy images of HepG2 cells treated with ZnPc(1.5%)/LDH with 0 h incubation and 24 h incubation (Figure S10).

Acknowledgment

This work was supported by the National Natural Science Foundation of China (NSFC), the 973 Program (Grant No.: 2014CB932104), the Scientific Fund from Beijing Municipal Commission of Education (20111001002) and the Fundamental Research Funds for the Central Universities (ZD 1303). M.W. appreciates the China National Funds for Distinguished Young Scholars of the NSFC. D.Y. thanks the China National Funds for Excellent Young Scholars of the NSFC.

Received: November 10, 2013
Revised: December 17, 2013
Published online: February 18, 2014

[1] a) A. Castano, P. Mroz, M. Hamblin, *Nat. Rev. Cancer* **2006**, *6*, 535; b) M. Wang, L. Huang, S. K. Sharma, S. Jeon, S. Thota, F. F. Sperandio, S. Nayka, J. Chang, M. Hamblin, L. Y. Chiang, *J. Med. Chem.* **2012**, *55*, 4274; c) M. J. Sailor, J. H. Park, *Adv. Mater.* **2012**, *24*, 3779.

[2] a) D. Dolmans, R. D. Fukumura, *Nat. Rev. Cancer* **2003**, *3*, 380; b) R. Dosselli, C. Tampieri, R. R. González, S. D. Munari, X. Ragàs, D. S. García, M. Agut, S. Nonell, E. Reddi, M. Gobbo, *J. Med. Chem.* **2013**, *56*, 1052; c) E. A. Rozhkova, *Adv. Mater.* **2011**, *23*, H136.

[3] a) M. Detty, S. Gibson, S. Wagner, *J. Med. Chem.* **2004**, *47*, 3897; b) S. Kimani, G. Ghosh, A. Ghogare, B. Rudshteyn, D. Bartusik, T. Hasan, A. Greer, *J. Org. Chem.* **2012**, *77*, 10638; c) H. L. Tu, Y. S. Lin, H. Y. Lin, Y. Hung, L. W. Lo, Y. F. Chen, C. Y. Mou, *Adv. Mater.* **2009**, *21*, 172.

[4] a) C. Fabris, G. Valduga, G. Miotto, L. Borsetto, G. Jori, S. Garbisa, E. Reddi, *Cancer Res.* **2001**, *61*, 7495; b) M. Velusamy, J. Y. Shen, J. T. Lin, Y. C. Lin, C. C. Hsieh, C. H. Lai, C. W. Lai, M. L. Ho, Y. C. Chen, P. T. Chou, J. K. Hsiao, *Adv. Funct. Mater.* **2009**, *19*, 2388.

[5] a) J. P. Celli, B. Q. Spring, I. Rizvi, C. L. Evans, K. S. Samkoe, S. Verma, B. W. Pogue, T. Hasan, *Chem. Rev.* **2010**, *110*, 2795; b) J. Morgan, A. Oseroff, *Adv. Drug Delivery Rev.* **2001**, *49*, 71; c) P. Zhang, W. Steelant, M. Kumar, M. Scholfield, *J. Am. Chem. Soc.* **2007**, *129*, 4526; d) C. Xing, L. Liu, H. Tang, X. Feng, Q. Yang, S. Wang, G. C. Bazan, *Adv. Funct. Mater.* **2011**, *21*, 4058.

[6] a) K. Lang, J. Mosinger, D. M. Wagnerová, *Coord. Chem. Rev.* **2004**, *248*, 321; b) A. E. O'Connor, W. M. Gallagher, A. T. Byrne, *Photochem. Photobiol.* **2009**, *85*, 1053; c) W. Liu, T. J. Jensen, F. R. Fronczek, R. P. Hammer, K. M. Smith, M. G. H. Vicente, *J. Med. Chem.* **2005**, *48*, 1033; d) N. Cauchon, M. Nade, G. Bkaily, J. E. Van Lier, D. Hunting, *Photochem. Photobiol.* **2006**, *82*, 1712.

[7] a) Y. N. Konan, R. Gurny, E. Allémann, *J. Photochem. Photobiol. B* **2002**, *66*, 89; b) I. Roy, T. Y. Ohulchanskyy, H. E. Pudavar, E. J. Bergey, A. R. Oseroff, J. Morgan, T. J. Dougherty, P. N. Prasad, *J. Am. Chem. Soc.* **2003**, *125*, 7860; c) Y. Cheng, A. C. Samia, J. D. Meyers, I. Panagopoulos, B. Fei, C. Burda, *J. Am. Chem. Soc.* **2008**, *130*, 10643.

[8] a) N. Nishiyama, Y. Morimoto, W. D. Jang, K. Kataoka, *Adv. Drug Delivery Rev.* **2009**, *61*, 327; b) M. Kuruppuarachchi, H. Savoie, A. Lowry, C. Alonso, R. W. Boyle, *Mol. Pharmaceutics* **2011**, *8*, 920; c) M. Mitsunaga, M. Ogawa, N. Kosaka, L. T. Rosenblum, P. L. Choyke, H. Kobayashi, *Nat. Med.* **2011**, *17*, 1685; d) M. Brasch, A. Escosura, Y. Ma, C. Uetrecht, A. J. R. Heck, T. Torres, J. J. L. M. Cornelissen, *J. Am. Chem. Soc.* **2011**, *133*, 6878; e) J. Shan, S. J. Budijono, G. Hu, N. Yao, Y. Kang, Y. Ju, R. K. Prud'homme, *Adv. Funct. Mater.* **2011**, *21*, 2488.

[9] a) H. Maeda, *Adv. Enzyme Regul.* **2001**, *41*, 189; b) K. Park, S. Lee, E. Kang, K. Kim, K. Choi, I. C. Kwon, *Adv. Funct. Mater.* **2009**, *19*, 1553; c) S. Lee, J. H. Ryu, K. Park, A. Lee, S. Y. Lee, I. C. Youn, C. H. Ahn, S. M. Yoon, S. J. Myung, D. H. Moon, X. Chen, K. Choi, I. C. Kwon, K. Kim, *Nano Lett.* **2009**, *9*, 4412; d) K. H. Min, K. Park, Y. S. Kim, S. M. Bae, S. Lee, H. G. Jo, R. W. Park, I. S. Kim, S. Y. Jeong, K. Kim, I. C. Kwon, *J. Controlled Release* **2008**, *127*, 208.

[10] a) B. A. Bench, A. Beveridge, W. M. Sharman, G. J. Diebold, J. E. Lier, S. M. Gorun, *Angew. Chem. Int. Ed.* **2002**, *41*, 748; b) S. Kim, T. Ohulchanskyy, H. Pudavar, R. Pandey, P. Prasad, *J. Am.*

Chem. Soc. **2007**, *129*, 2669; c) Z. Yan, H. Xu, S. Guang, X. Zhao, W. Fan, X. Y. Liu, *Adv. Funct. Mater.* **2012**, *22*, 345; d) S. Bonneau, C. V. Bizer, *Expert Opin. Ther. Pat.* **2008**, *18*, 1011; e) H. Mojzisova, S. Bonneau, D. Brault, *Eur. Biophys. J.* **2007**, *36*, 943.

[11] a) G. Hu, D. O'Hare, *J. Am. Chem. Soc.* **2005**, *127*, 17808; b) A. M. Fogg, V. M. Green, H. G. Harvey, D. O'Hare, *Adv. Mater.* **1999**, *11*, 1466; c) U. Costantino, M. Nocchetti, R. Vivani, *J. Am. Chem. Soc.* **2002**, *124*, 8428; d) J. A. Gursky, S. D. Blough, C. Luna, C. Gomez, A. N. Luevano, E. A. Gardner, *J. Am. Chem. Soc.* **2006**, *128*, 8376; e) J. W. Boclair, P. S. Braterman, *Chem. Mater.* **1999**, *11*, 298.

[12] a) J. H. Choy, S. Y. Kwak, J. S. Park, Y. J. Jeong, J. Portier, *J. Am. Chem. Soc.* **1999**, *121*, 1399; b) M. Darder, P. Aranda, E. R. Hitzky, *Adv. Mater.* **2007**, *19*, 1309; c) E. R. Hitzky, M. Darder, P. Aranda, K. Ariga, *Adv. Mater.* **2010**, *22*, 323; d) M. Shao, F. Ning, J. Zhao, M. Wei, D. G. Evans, X. Duan, *J. Am. Chem. Soc.* **2012**, *134*, 1071; e) M. Q. Zhao, Q. Zhang, J. Q. Huang, F. Wei, *Adv. Funct. Mater.* **2012**, *22*, 675.

[13] a) W. Shi, S. He, M. Wei, D. G. Evans, X. Duan, *Adv. Funct. Mater.* **2010**, *20*, 3856; b) S. Li, J. Lu, M. Wei, D. G. Evans, X. Duan, *Adv. Funct. Mater.* **2010**, *20*, 2848; c) D. P. Yan, J. Lu, J. Ma, M. Wei, D. G. Evans, X. Duan, *Angew. Chem. Int. Ed.* **2010**, *49*, 720; d) D. P. Yan, J. Lu, J. Ma, S. Qin, M. Wei, D. G. Evans, X. Duan, *Angew. Chem. Int. Ed.* **2011**, *50*, 7037; e) D. P. Yan, S. H. Qin, L. Chen, J. Lu, J. Ma, M. Wei, D. G. Evans, X. Duan, *Chem. Commun.* **2010**, *46*, 8654.

[14] F. Camerel, J. Barbera, J. Otsuki, T. Tokimoto, Y. Shimazaki, L. Y. Chen, S. H. Liu, M. S. Lin, C. C. Wu, R. Ziessel, *Adv. Mater.* **2008**, *20*, 3462.

[15] K. M. Kadish, K. M. Smith, R. Guilard, Handbook of Porphyrin ScienceWorld Scientific, Singapore **2010**.

[16] a) K. Yang, H. Xu, L. Cheng, C. Sun, J. Wang, Z. Liu, *Adv. Mater.* **2012**, *24*, 5586; b) P. Huang, J. Lin, X. Wang, Z. Wang, C. Zhang, M. He, K. Wang, F. Chen, Z. Li, G. Shen, D. Cui, X. Chen, *Adv. Mater.* **2012**, *24*, 5104.

[17] a) W. Spiller, H. Kliesch, D. Wohrele, S. Hackbarth, B. Roder, G. J. Schnurpfeil, *J. Porphyrins Phthalocyanines* **1998**, *2*, 145; b) D. B. Tada, L. L. R. Vono, E. L. Duarte, R. Itri, P. K. Kiyohara, M. S. Baptista, L. M. Rossi, *Langmuir* **2007**, *23*, 8194.

[18] C. Wang, L. Cheng, Y. Liu, X. Wang, X. Ma, Z. Deng, Y. Li, Z. Liu, *Adv. Funct. Mater.* **2013**, DOI: 10.1002/adfm.201202992.